Morphological Features and Melting Behavior of Nanocomposites Based on Isotactic Polypropylene and Multiwalled Carbon Nanotubes

Carlos A. Avila-Orta,[1] Francisco J. Medellín-Rodríguez,[2] Mario V. Dávila-Rodríguez,[1,3] Yrayda A. Aguirre-Figueroa,[1,3] Kyunghwan Yoon,[4] Benjamin S. Hsiao[4]

[1]*Departamento de Materiales Avanzados. Centro de Investigación en Química Aplicada, Blvd. Enrique Reyna H. No. 140, Saltillo, Coah 25253, México*
[2]*CIEP/FCQ. Universidad Autónoma de San Luis Potosí, Dr. Manuel Nava No. 6, San Luis Potosí SLP 78210, México*
[3]*Instituto Tecnológico de Saltillo, Blvd. Venustiano Carranza No. 2400, Saltillo, Coah 25280, México*
[4]*Department of Chemistry. Stony Brook University, Stony Brook, NY 11794-3400, USA*

Received 4 April 2006; accepted 6 May 2007
DOI 10.1002/app.26823
Published online 30 July 2007 in Wiley InterScience (www.interscience.wiley.com).

ABSTRACT: Nanocomposites based on low molar mass isotactic polypropylene (iPP) and a low concentrations (1–2 wt %) of multiwalled carbon nanotubes (MWCNTs) were studied using thermal analysis, optical and electronic microscopy, and X-ray diffraction/scattering techniques. It was first determined that MWCNT decrease induction time and act as nucleating agents of the iPP crystals during nonisothermal crystallization. One of the consequences of the nucleation effect was that the original spherulitic morphology of iPP was transformed into a fibrillar-like. The corresponding long period of the original well-defined lamellar structure slightly increased suggesting the formation of thicker crystals in samples containing MWCNT. The nature of the α-iPP crystalline structure was not affected by MWCNT. After nonisothermal crystallization, two melting endotherms were present during thermal scanning of the iPP/MWCNT nanocomposites their proportion changing with the heating rate. After resolving the total DSC signal in its components using MDSC, the overall evolution of such behavior could be explained in terms of the melting/recrystallization mechanism. © 2007 Wiley Periodicals, Inc. J Appl Polym Sci 106: 2640–2647, 2007

Key words: morphology; crystallization; melting

INTRODUCTION

Polymer nanocomposites containing dispersed nanoparticles are a new important class of materials.[1–4] Among the different nanoaditives available up to date, one-dimensional nanoparticles, such as carbon nanotubes (CNTs),[5] are especially attractive because they can improve a number of properties once integrated within the polymeric matrix. Both the dispersion of CNT and the molecular interactions between CNT and the polymeric matrix are two important factors which will dictate the final properties of the polymeric nanocomposite. These two factors can be controlled by functionalizing[6] the nanotube surface and by solution mixing or melt blending although a better CNT dispersion is often obtained by using solution mixing rather than melt blending. In solution mixing, the small solvent molecules can penetrate easily and break down the CNT agglomerates, effect that is difficult to obtain by melt blending. Nonetheless, the latter is preferred for practical purposes.

In this study, we are particularly interested in thermoplastic nanocomposites containing isotactic polypropylene (iPP) and multi-walled carbon nanotubes (MWCNT). There have been several studies regarding mechanical performance,[7,8] electrical properties,[9,10] and decomposition[11,12] of this polymeric system, although the experimental results fall short from theoretical predictions. It is also well known that the physical properties of polymers are intimately linked to the morphology, which is developed after thermal and mechanical treatments. Therefore, morphological factors may help to tailor the properties of the iPP/MWCNT nanocomposites. Grady et al.[13] observed for example that octadecylamide-functionalized single-walled carbon nanotubes (SWCNT) promote the formation of β-iPP crystals. These authors determined the existence of β-iPP crystals from the melting behavior of iPP/SWCNT nanocomposites. Contrastingly, a number of studies show that SWCNT[14] and MWCNT[10,15] promote the formation of α-iPP crystals. It has also been reported

Correspondence to: C.A. Avila-Orta (cavila@ciqa.mx).
Contract grant sponsor: Centro de Investigación en Química Aplicada; contract grant number: F70601.
Contract grant sponsor: US Department of Energy; contract grant number: DE-FG02-99ER 45760.

that iPP/MWCNT nanocomposites exhibit fibrillar rather than spherulitic morphology,[15] and that the Avrami exponent decreases with the nanotubes concentration,[16,17] although in these studies the molar mass of the iPP matrix was within an intermediate commercial range. In the present study, low molecular weight iPP was used to produce well-dispersed nanocomposites assuming that short polymer chains may easily penetrate and break apart CNTs agglomerates. Under these circumstances, the overall purpose of this study was to determine the effect of MWCNT on the crystallization, morphology, and melting behavior of iPP.

EXPERIMENTAL

Materials

Low molecular weight iPP (grade 42,811-6) was obtained from Aldrich, the weight-average molecular weight M_w was 12,000 g/g mol. MWCNT were obtained from NanoLab, they were graded PD15L15 with a reported external diameter of 15 ± 5 nm, inner diameter of 7 ± 2 nm, length of 1–5 μm, and purity higher than 95% (the impurity residuals include iron, cobalt, and nickel).

Nanocomposites preparation

To generate an intimate mixing of the components,[18–20] iPP/MWCNT nanocomposites with up to 2 wt % of MWCNT were prepared in xylene solution.[20] For this purpose, both components were mixed in xylene at 120°C during a 1 h period and then the suspension was precipitated in cold methanol. The precipitated powder was filtrated and vacuum dried at 50°C during 4 h. The resulting nanocomposites in powder form were melted at 190°C for 3 min in a Metller FP82HT using a stainless steel mold and then they were cooled down to room temperature (RT) at a cooling rate of −5°C/min.

Conventional and modulated DSC

Differential scanning calorimetry (DSC) thermal traces of iPP/MWCNT nanocomposites were obtained in a DSC 2920 TA instruments experimental equipment. All thermal traces were obtained under nitrogen atmosphere. Temperature and heat flow were calibrated using the indium standard. The complex heat capacity (C_p) in the modulated DSC (MDSC) was calibrated using a sapphire standard. All samples were first melted at 190°C for 3 min in the DSC and then they were cooled down to RT at a cooling rate of −5°C/min. The samples were then heated at different heating rates 2, 5, and 10°C/min up to the melting temperature to determine the melting behavior. A modulation of 0.318°C every 60 s was used in MDSC for the underlying heating rate of 2°C/min. A similar modulation treatment proved to be effective for determination of melting behavior during heating of iPP.[21]

Simultaneous SAXS and WAXD measurements

Simultaneous small-angle X-ray scattering (SAXS) and wide-angle X-ray diffraction (WAXD) measurements were carried out at the X27C beamline in the National Synchrotron Light Source (NSLS) (Brookhaven National Laboratory (BNL), NY, USA). Samples were first melt prepared into a disk-shape form with a diameter of 5 mm and average thickness of 1.5 mm. These specimens were then placed inside a copper holder covered with two Kapton windows, and the assembly was inserted into a Mettler hot-stage (FP-82HT). Samples were first melted at 190°C for 3 min and then cooled down to RT at a cooling rate of −5°C/min. Simultaneous SAXS/WAXS patterns were collected after the cooling process at RT. The wavelength (λ) was 1.371 Å. The sample-to-detector distance for the SAXS measurements was 1850.3 and for the WAXD portion 106.8 mm. Two different bidimensional X-ray detectors were used for data collection, MAR-CCD for SAXS and FUJI imaging plates for WAXD. A BAS-2500 scanner was used to extract the digital image from the imaging plate. The bidimensional SAXS/WAXD images were converted to linear intensity profiles as a function of the scattering vector, $s = 2/\lambda \sin \theta$ (where λ is the wavelength and θ is half of the scattering angle), through a circular averaging method. All intensity profiles were corrected for beam fluctuations and background scattering.

Polarized optical microscopy/scanning electron microscopy

The morphology of iPP/MWCNT was obtained using polarized optical microscopy (POM) and scanning electron microscopy (SEM). In the former, a small portion of the sample was sandwiched between two thin glass covers and melted at 190°C for 3 min in a Mettler hot stage (FP-82HT). This was attached to an optical microscope (Olympus BX60) equipped with digital image acquisition. The sample was then cooled down to RT at a cooling rate of −5°C/min. Sequential images were then obtained at different temperatures during the nonisothermal crystallization process. SEM specimens were subjected to the same thermal treatments as indicated before although without using surface covering. In this particular case, the sample surface was not metal etched. SEM images were taken on the uncovered surface using a TOP-CON SM-510 scanning electron microscope with a working voltage of 15 kV.

RESULTS AND DISCUSSION

Nonisothermal crystallization

In many practical applications, thermoplastic semicrystalline polymers are often cooled from the molten state to RT at high cooling rates; therefore, as a result of the cooling process, nonisothermal crystallization occurs. In this study, the thermal effect of MWCNT on the nonisothermal crystallization process was determined through DSC, although the cooling rates used were far from the actual conditions. Typical crystallization exotherms, which were obtained during controlled cooling from the melt of iPP and iPP/MWCNT nanocomposites, are shown in Figure 1. Here, the total heat released during the nonisothermal crystallization process (ΔH_c) was obtained from the integration of the area under the crystallization exotherms and it is shown in Table I. The results indicate that the total heat released during crystallization slightly change with the MWCNT content. Taking as a reference the heat of fusion of 100% crystalline iPP (ΔH_f = 209 J/g),[22] the iPP crystalline fraction X_c developed by the nanocomposites was calculated using the formula: $X_c = \Delta H_c/\Delta H_f$. The results are presented in Table I and indicate that the crystalline fraction remains practically constant with the increase in MWCNT content. On the other hand, it is observed that the crystallization onset temperature (T_{on}) also shifts to higher values with the increase in MWCNT (see Table I). The increase in T_{on}, at a fixed cooling rate, indicates a decrease in the crystallization induction temperature (or induction time) of iPP in the presence of MWCNT. This is an evidence of the enhancement of heterogeneous nucleation since the time to form the critical nucleus has been diminished. This effect has been reported in polymeric systems containing both SWCNT[13,14,16,17] and MWCNT.[10,15]

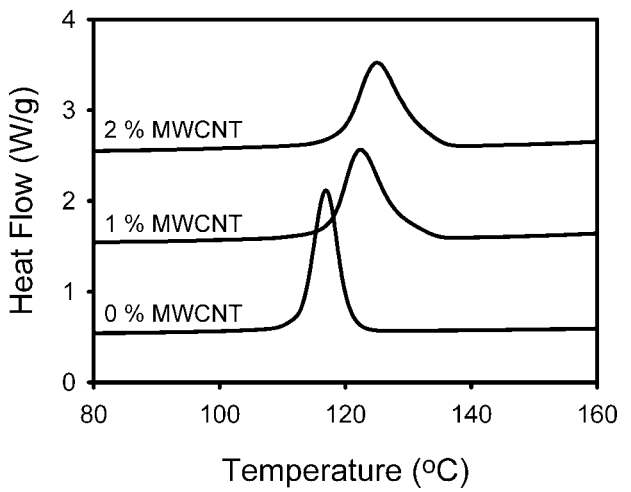

Figure 1 DSC cooling traces of iPP/MWCNT nanocomposites during nonisothermal crystallization from the melt. The cooling rate was 5°C/min.

TABLE I
Crystallization Parameters for Nonisothermal Crystallization of iPP/MWCNT Nanocomposites with Different MWCNT Content (Cooling rate 5°C/min)

% MWCNT	T_{on} (°C)	t_{on} (s)	ΔH_c (J/g)	X_c	L (nm)
0	120.6	832.8	99.6	0.47	13.8
1	129.3	728.4	101.4	0.48	17.8
2	132.5	690.0	103.5	0.49	16.0

A consequence of the heterogeneous nucleation process was the induction of changes in the overall morphology. *In situ* micrographs of neat iPP and iPP/MWCNT nanocomposites were taken during the nonisothermal crystallization process at 120°C and the results are shown in Figure 2. It is necessary to mention that the indicated temperature is immediately after the onset of crystallization of neat iPP, while in the case of the sample with 2 wt % MWCNT the crystallization process is almost complete at such temperature (see Fig. 1). In the results of Figure 2, the typical spherulitic morphology is observed in neat iPP [Fig. 2(a)]. This was not the case however with the sample containing 2 wt % MWCNT and whose results are shown in Figure 2(b,c). Here, rather distorted crystals are observed in the POM micrographs which would not allow however to discard the possibility of having immature spherulites in the morphology. Therefore, to gain insight on the nature of the latter crystals, SEM micrographs of iPP/MWCNT (98/2 wt %) were taken at different magnifications and the results are shown in Figure 3(a,b). It is indeed observed in these results that a fibrillar-like structure is now characteristic of the crystallized samples containing 2 wt % MWCNT. The same type of morphology has been reported before by Assouline[15] in iPP/MWCNT nanocomposites.

The origin of the fibrillar structures in iPP/MWCNT nanocomposites has not yet been explained[14,15] although some possibilities include transcrystallinity through contraction/wetting of the polymer.[15] In recent studies, Li et al.[23,24] proposed that PE crystals decorate SWCNT, MWCNT, and CNF through a size-dependent epitaxy mechanism. This results in nanohybrid shish–kebab (NHSK) structures. It is well known that flow-induced crystallization also induces shish–kebab polymer morphology,[25] however, in the absence of flow conditions, Li et al.[23,24] have demonstrated that SWCNT, MWCNT, and CNF act as the central fibril core (shish) while the kebabs are formed by disc-shaped lamellar polymer crystals.

To study potential changes in the lamellar structure of iPP induced by the presence of MWCNT, SAXS data were collected from isotropic crystalline

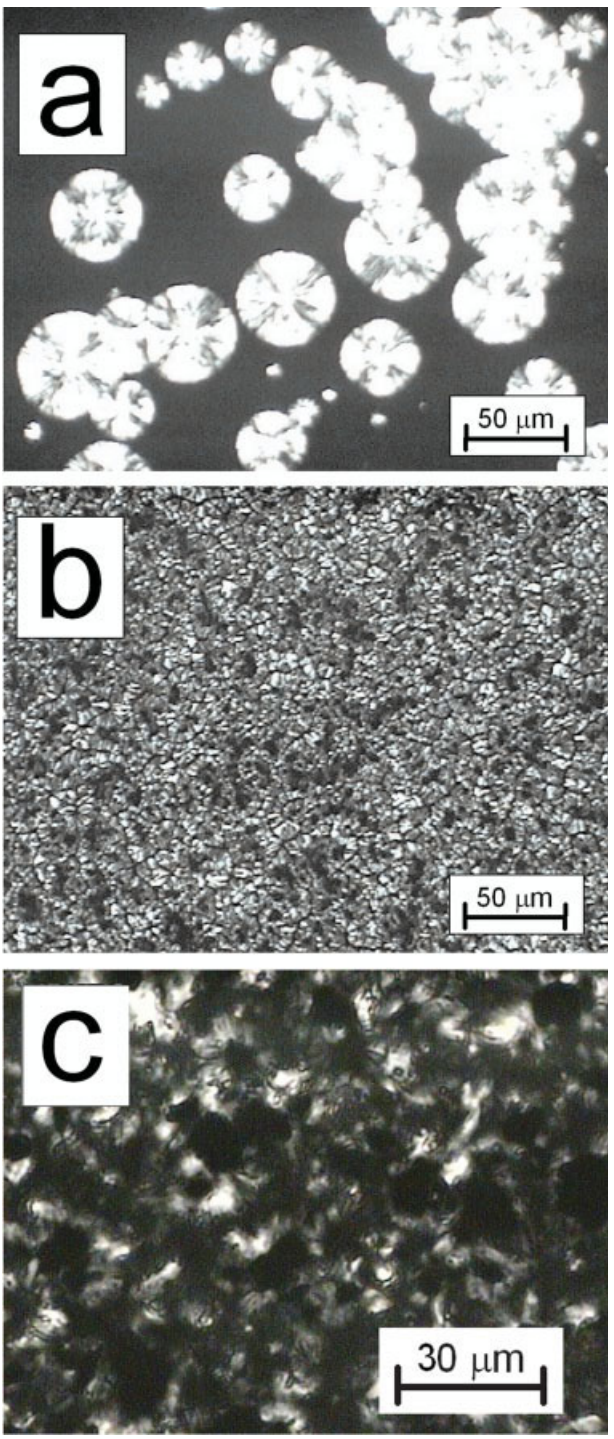

Figure 2 POM micrographs at 120°C on cooling from the melt at a cooling rate of 5°C/min: (a) neat iPP, (b) iPP/MWCNT (98/2 wt %), (c) ipp/MWCNT (98/2 wt %).

samples. 2D intensity patterns and 1D SAXS profiles of iPP and iPP/MWCNT polymer nanocomposites are shown in Figure 4. The 2D SAXS patterns of samples with 2 wt % MWCNT did not show any preferred orientation (see the inset in Fig. 4), confirming the overall random orientation of polymer crystals. Figure 4 also indicates that the scattering

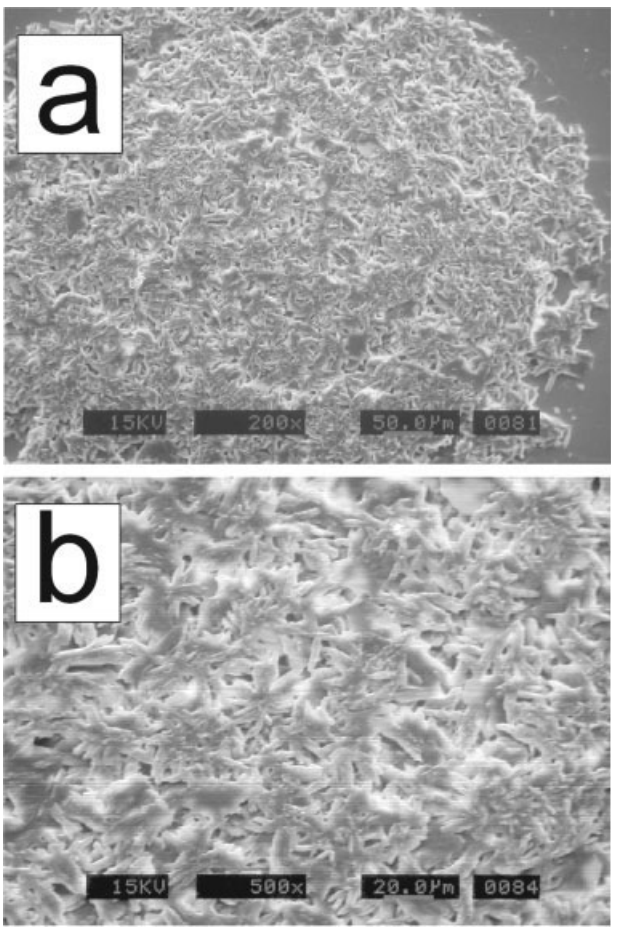

Figure 3 SEM micrographs of iPP/MWCNT (98/2 wt %) after nonisothermal crystallization from the melt: (a) 200×, (b) 500×.

maximum of the intensity profiles is less defined for samples containing MWCNT, indicating that the lamellar packing becomes less regular. The long

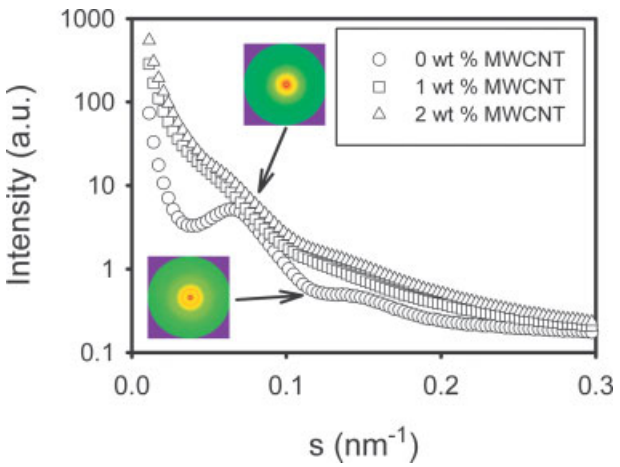

Figure 4 One-dimensional SAXS intensity profiles of neat iPP and iPP/MWCNT nanocomposites after nonisothermal crystallization from the melt. The inset shows the 2D SAXS profiles for the indicated samples. [Color figure can be viewed in the online issue, which is available at www.interscience.wiley.com.]

period, $L = 1/s_{max}$, was calculated from the SAXS results. Here s_{max} corresponds to the scattering maximum in the Lorentz-corrected intensity profiles (Fig. 5). It was determined that L increases slightly with the MWCNT content (see the results in Table I). An increase in the long period usually comes from an increase in lamellar thickness which also corresponds to a higher melting point. However, in this particular study we have to correlate the results with the observed double melting behavior as will be discussed later.

The crystal structure of neat iPP and iPP/MWCNT nanocomposites, nonisothermally crystallized from the melt, was determined at RT using X-ray diffraction and the results are shown in Figure 6. It is observed that in both, iPP and iPP/MWCNT, α-iPP crystals predominate.[15] Previous studies have indicated that octadecylamine functionalized SWCNT[13] nucleate β-iPP crystals. However, our results and some others[10,14,15] are not in agreement with this observation. We have to mention, however, that the CNTs used in this study were only purified and in addition the preparation methods melt blending,[10,14] and spin-coating after solution mixing,[15] were different than those of functionalized iPP.[13] Therefore, most probably the functionalization of CNTs and/or the preparation method results in different crystal habits.

Melting behavior

The melting behavior of the nonisothermally crystallized specimens is shown in Figure 7. In the case of neat iPP, the melting behavior is characteristic of low molecular weight species.[26,27] The two melting endotherms observed were labeled as I and II (with peak temperatures $T_{m,I}$ and $T_{m,II}$) depending on their

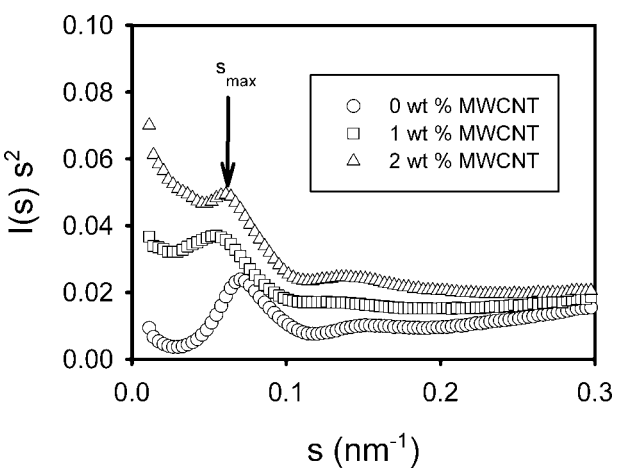

Figure 5 Lorentz corrected plot of neat iPP and iPP/MWCNT nanocomposites after nonisothermal crystallization from the melt.

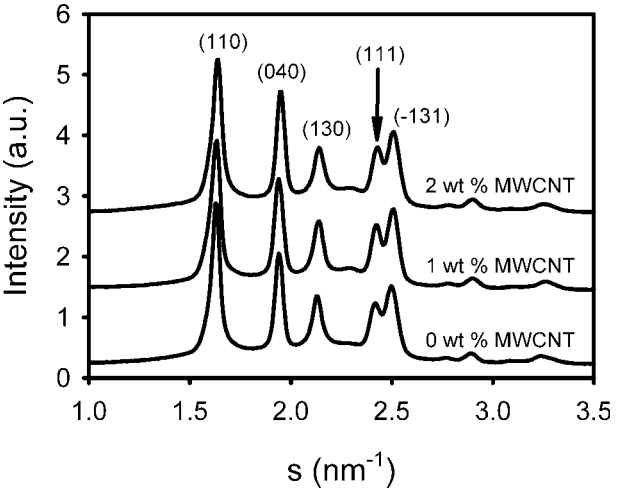

Figure 6 One-dimensional WAXD intensity profiles of near iPP and iPP/MWCNT nanocomposites after nonisothermal crystallization from the melt.

sequential appearance although the crystallinity degree slightly increased compared with the crystallization process (see Table II). The double melting behavior of α-iPP has been explained in terms of[28]: (1) melting of two different crystal populations and (2) the melting–recrystallization–melting mechanism. In the latter case, perfecting of the less stable original crystallites is assumed to take place during linear heating leading to the appearance of a second higher melting endotherm.[29] Such recrystallization process depends on both time and temperature, therefore, increasing the heating rate leads to a decrease of the second melting endotherm since there is less time for recrystallization to occur. In agreement with this hypothesis, the melting behavior of neat iPP in Figure 7 indicates that endotherm I grows at expenses of endotherm II with an increase in the heating rate. The contribution of endotherm II to the melting process of iPP becomes significantly reduced at a heating rate of 10°C/min, indicating that the polymer crystals have less time to recrystallize. In this case, we consider a population of lamellar crystals formed prior to the heating scan that melt at low temperature (endotherm I), while the high-temperature second endotherm is assigned to melting of the recrystallized crystals. A similar effect was observed in the case of iPP/MWCNT nanocomposites, with 1 and 2 wt % MWCNT. Here, the low melting endotherm grows at expense of the high melting endotherm, suggesting again that the second melting endotherm is due to the melting of recrystallized crystals. This effect is more pronounced for samples with 2 wt % MWCNT, indicating that MWCNT inhibit the recrystallization process during heating, therefore, only one melting endotherm I is observed at a heating rate of 10°C/min. We have to mention that in some

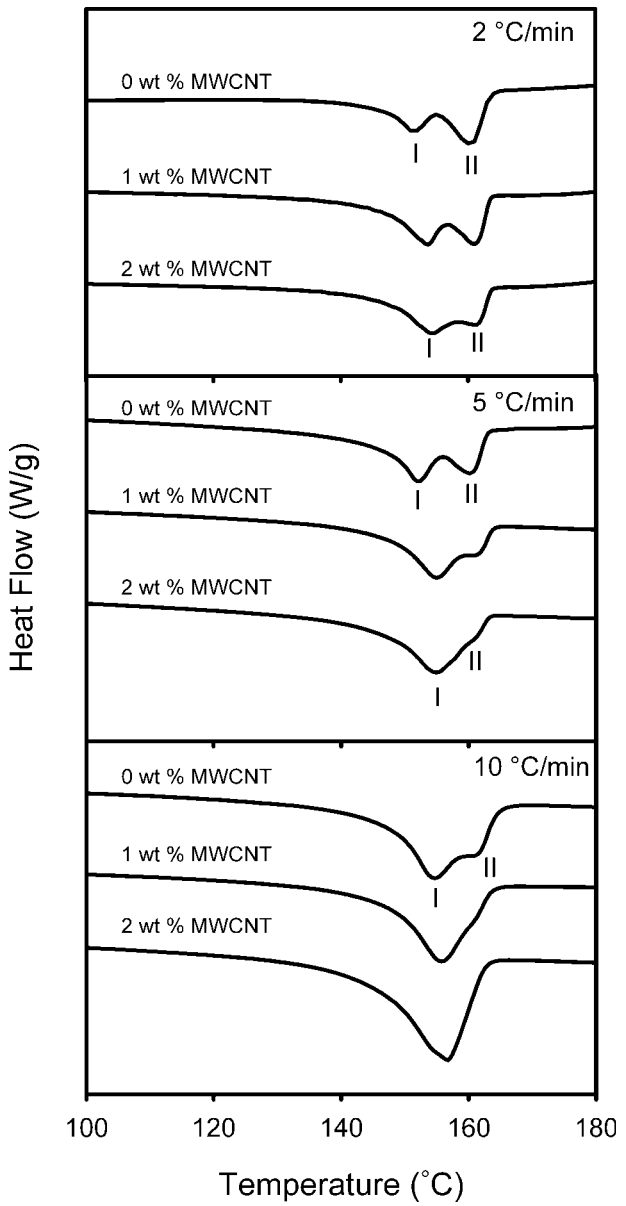

Figure 7 DSC heating traces at different heating rates of neat iPP and iPP/MWCNT nanocomposites nonisothermally crystallized from the melt. Heating rates: 2°C/min, 5°C/min, and 10°C/min. The CNTs content is shown.

other high-temperature neat polymeric two phase systems, there exists primary and secondary crystallization whose nature can range within a number of possibilities and so can do the proposed crystallization and melting mechanisms. These polymeric systems were also first considered within the context of the melting–recrystallization mechanism until new evidences were given to explain their complex behavior. Currently, there is not enough experimental evidence as for supporting a different mechanism in iPP and in the MWCNT nanocomposites.

Variations of heating rates are frequently used to support the recrystallization hypothesis, although another alternative for this last purpose is to use MDSC.[21,30] This experimental technique was first introduced by Reading in 1993.[31] In MDSC, a sinusoidal temperature oscillation (modulation) is overlaid on the conventional linear temperature ramp. Then, the total heat flow is the result of two components, one depends only on the absolute temperature (kinetic component), and the other is heating rate dependent (thermodynamic or heat capacity component). MDSC can differentiate thermodynamic and kinetic events by splitting the total signal into the reversible and nonreversible components.[31] Thermodynamic events are associated with the reversing signal, while the nonreversing signal is associated with both thermodynamic and kinetic events. Conventional and MDSC heating experiments of nonisothermally crystallized iPP and iPP/MWCNT (2 wt %) are shown in Figure 8. Here, it is shown that that the total conventional DSC resembles the total MDSC trace at 2°C/min and two melting endotherms are observed in both cases although in different proportions. The total signal of neat iPP splits into a double melting reversing signal and a recrystallization/melting nonreversing signal as shown in Figure 9(a). However, in spite of the existence of the two melting endotherms in the total signal of the nanocomposite, the recrystallization exotherm was

TABLE II
Melting Parameters of iPP/MWCNT Nanocomposites with Different MWCNT Content Nonisothermally Crystallized from the Melt (Heating Rate 5°C/min)

% MWCNT	$T_{m,I}$ (°C)	$T_{m,II}$ (°C)	X_c
0	151.5	160.3	0.52
1	153.8	160.0	0.53
2	154.7	160.3	0.54

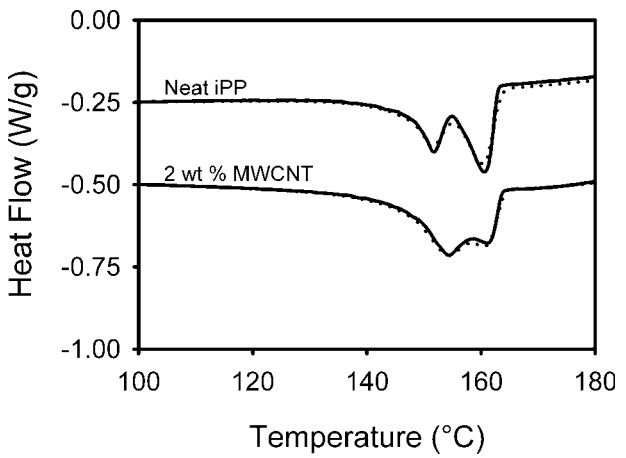

Figure 8 Total DSC traces at 2°C/min of neat and nanocompounded iPP obtained in conventional (solid line) and modulated mode (dotted line). A modulation of ±0.318°C, 60 s was used in modulated measurements.

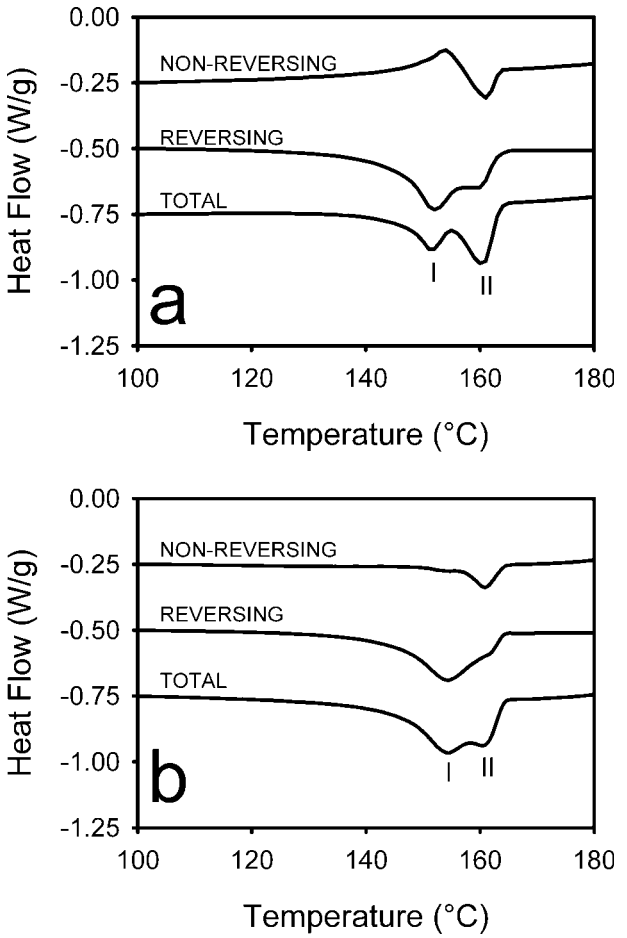

Figure 9 MDSC heating traces of (a) neat iPP and (b) iPP/MWCNT (98/2% wt) nonisothermally crystallized from the melt. The underlying heating rate was 2°C/min, ±0.318°C, 60 s.

not present for the sample containing 2 wt % of MWCNT [Fig. 9(b)]. Therefore, we can conclude that the presence of MWCNT decreased recrystallization during melting, most probably due to the formation of thicker less regularly overall packed crystals. This possibility was considered by other authors when iPP was loaded with talc, an inorganic fillers.[28] Although not proved here, the melting behavior could involve the presence of thicker epitaxialy grown α-form iPP crystals as suggested by other authors.[15,23]

CONCLUSIONS

The effect of MWCNT on the crystallization, morphology, and melting behavior of a low molecular weight iPP has been studied. The induction time for crystallization decreased with the addition of MWCNT. Therefore, MWCNT acted as nucleating agents for iPP α-crystals even though the crystalline fraction of iPP remained practically constant with MWCNT content. The heterogeneous nucleation process of iPP on MWCNT motivated a morphological change from typical spherulitic form to a fibrillar-like structure. The Lorentz-corrected long period increased slightly although the lamellar packing became less regular. Two melting endotherms were observed during heating of neat iPP and iPP/MWCNT nanocomoposites. The low melting temperature endotherm I was associated to the melting of crystals formed during the nonisothermal crystallization process, while the high melting temperature endotherm was associated with melting of crystals formed during the heating scan (recrystallized crystals). The double melting behavior of the iPP/MWCNT nanocomposites could be explained on the basis of the melting–recrystallization–melting mechanism. The decrease in recrystallization of α-iPP crystals heterogeneously nucleated on MWCNT was probably due to the formation of less regularly packed, but more stable (probably thicker), crystals which melted at a slightly higher ($T_{m,I}$) temperature with the increase in MWCNT.

This work was supported by the project CIQA-F70601. The authors acknowledge the experimental work of B.M. Huerta-Martínez and J.L de la Peña, both from CIQA. The synchrotron X-ray experiments were carried out in the National Synchrotron Light Source, Brookhaven National Laboratory, USA.

References

1. Alexandre, M.; Dubois, P. Mater Sci Eng 2000, 28, 1.
2. Thostensona, E. T.; Renb, Z.; Choua, T.-W. Compos Sci Technol 2001, 61, 1899.
3. Andrews, R.; Weisenberger, M. C. Curr Opin Solid State Mater Sci 2004, 8, 31.
4. Khare, R.; Bose, S. J Miner Mater Char Eng 2005, 4, 31.
5. Ijima, S. Nature 1999, 354, 56.
6. Hirsch, A. Angew Chem Int Ed 20l02, 41, 1853.
7. Kearns, J. C.; Shambaugh, R. L. J Appl Polym Sci 2079 2002, 86.
8. Moore, E. M.; Ortiz, D. L.; Marla, V. T.; Shambaugh, R. L.; Grady, B. P. J Appl Polym Sci 2004, 93, 2926.
9. Seo, M.-K.; Park, S.-J Chem Phys Lett 2004, 395, 44.
10. Seo, M.-K.; Lee, J.-R.; Park, S.-J. Mater Sci Eng A Struct 2005, 404, 79.
11. Kashiwagi, T.; Grulke, E.; Hilding, J.; Harris, R.; Awad, A.; Douglas, J. Macromol Rapid Commun 2002, 23, 761.
12. Kashiwagi, T.; Grulke, E.; Hilding, J.; Groth, K.; Harris, R.; Butler, K.; Shields, J.; Kharchenko, S.; Douglas, J. Polymer 2004, 45, 4227.
13. Grady, B. P.; Pompeo, F.; Shambaugh, R. L.; Resasco, D. E. J Phys Chem B 2002, 106, 5852.
14. Bhattacharyya, A. P.; Sreekumar, T. V.; Liu, T.; Kumar, S.; Ericson, L. M.; Hauge, H.; Smalley, R. E. Polymer 2003, 44, 2373.
15. Assouline, E.; Lustiger, A.; Barber, A. H.; Cooper, C. A.; Klein, E.; Wachtel, E.; Wagner, H. D. J Polym Sci Part B: Polym Phys 2003, 41, 520.
16. Valentini, L.; Biagiotti, J.; Kenny, J. M.; Santucci, S. J Appl Polym Sci 2003, 87, 708.
17. Valentini, L.; Biagiotti, J.; López-Manchado, M. A.; Santucci, S.; Kenny, J. M. Polym Eng Sci 2004, 44, 303.

18. Seki, M.; Thurman, D. W.; Oberhauser, J. P.; Kornfield, J. A. Macromolecules 2002, 35, 2583.
19. Ran, R.; Burger, C.; Sics, I.; Yoon, K.; Fang, D.; Kim, K.; Avila-Orta, C.; Keum, J.; Chu, B.; Hsiao, B. S.; Cookson, D.; Shultz, D.; Lee, M.; Viccaro, J.; Otha, Y. Colloid Polym Sci 2004, 282, 802.
20. Avila-Orta, C. A.; Burger, C.; Somani, R.; Yang, L.; Marom, G.; Medellín-Rodríguez, F. J.; Hsiao, B. S. Polymer 2005, 46, 8859.
21. Ramírez-Vargas, E.; Navarro-Rodríguez, D.; Huerta-Martínez, B. M.; Avila-Orta, C. A.; Palacios-Mezta, M.; Medellín-Rodríguez, F. J. Int J Polym Mat 2002, 51, 485.
22. Bai, F.; Li, F.; Clahoun, B. H.; Quirk, R. P.; Cheng, S. Z. D. In Polymer Handbook, 4th ed. Brandrup, J.; Immergut, E. H.; Grulke, E. A., Eds. Wiley-Interscience: USA, 1999; Vol. 1, Chapter V.
23. Li, C. Y.; Li, L.; Cai, W.; Kodjie, S. L.; Tenneti, K. K. Adv Mater 2005, 17, 1198.
24. Li, L.; Li, C. Y.; Ni, Ch. J Am Chem Soc 2006, 128, 1692.
25. Keller, A.; Kolnaar, H. W. H. Mater Sci Technol 1997, 18, 189.
26. Morrow, D. R.; Newman, B. A. J Appl Phys 1968, 39, 4944.
27. Mandelkern, L. In Crystallization of Polymers, 2nd ed. Cambridge University Press: Cambridge, UK, 2002; Vol. 1, Chapter 2.
28. Varga, J. In Polypropylene. Structure, Blends and Composites, Karger-Kocsis, J., Ed. Chapman and Hall, Cambridge, Great Britain, 1995; Vol. 1, Chapter 3
29. Roberts, R. C. Polym Lett 1970, 8, 381.
30. Avila-Orta, C. A.; Medellín-Rodríguez, F. J.; Wang, Z.-G.; Navarro-Rodríguez, D.; Hsiao, B. S., Yeh, F. Polymer 2003, 44, 1527.
31. Reading, M. Trends Polym Sci 1993, 1, 248.